


## Property prediction of AZ80 magnesium alloy: an extreme learning machine model optimized by a new improved sparrow search algorithm

Pengju Zhang<sup>1,2</sup> , Jianping Zhang<sup>2</sup>, Jian Fu<sup>3,4</sup>, Wenbo Guo<sup>2</sup>, Dawen Zhao<sup>5</sup>, Liquan Wang<sup>1</sup>

<sup>1</sup>Harbin Engineering University, College of Mechanical and Electrical Engineering. 150001, Harbin, China.

<sup>2</sup>University of Shanghai for Science and Technology, School of Mechanical Engineering. 200093, Shanghai, China.

<sup>3</sup>Shanghai Electric Power Co. 200000, Shanghai, China.

<sup>4</sup>Shanghai Donghai Wind Power Generation Co. 200090, Shanghai, China.

<sup>5</sup>Shanghai Electric Wind Power Group Co. 200235, Shanghai, China.

e-mail: zhangpengjuusst@163.com, jpzhanglzu@163.com, fujianusst@163.com, wbguousst@163.com, zhaodawenusst@163.com, wangliquanhrbeu@163.com

### ABSTRACT

The mechanical properties of magnesium alloy in different molding stages are very important factors to determine its application approaches in engineering. In order to ensure the prediction accuracy of mechanical properties, a TCMSSA-ELM model, which is a hybrid of the sparrow search algorithm (SSA) optimized by the tent chaotic mapping (TCM) algorithm and the extreme learning machine (ELM), is proposed in this study, and the stresses of AZ80 magnesium alloy are predicted by the model through a 812-record dataset. The predicting results indicate that TCMSSA improves the accuracy of ELM model. Compared with ELM model, the data points formed by experimental values of stress and the predicted ones by TCMSSA-ELM model are closer to the ideal 45° line, the average determination coefficient rises by 1.43%, and the average root mean squared error (RMSE) decreases by nearly 61.96%, implying that TCMSSA-ELM model accurately reflects the influence rule of thermodynamic parameters on stress. The novelty of this study is that TCM is used to optimize the population initialization of SSA, which enables SSA to have a higher global search ability, and thus optimizes the weight and threshold selection of ELM, then making TCMSSA-ELM have higher prediction accuracy than other improved ELM models.

**Keywords:** Sparrow search algorithm; Extreme learning machine; TCMSSA-ELM model; AZ80 magnesium alloy; Mechanical property prediction.

### 1. INTRODUCTION

Magnesium alloy is one of the lightest structural materials in the manufacturing industry [1, 2]. It demonstrates such advantages as high specific stiffness, environmental protection, easy recycling, and also shows good electromagnetic shielding characteristics and shock absorption performance [3–5], which makes it widely applicable in various fields like aviation, aerospace, automobile and medicine [6, 7]. Classed as the high-strength Mg-Al-Zn wrought magnesium alloys, AZ80 magnesium alloy possesses outstanding mechanical properties such as strong oxidation resistance [8] and excellent welding performance [9, 10]. In recent years, there have been many studies focusing on AZ80 magnesium alloy to explore its performance, manufacture and application in large-scale support beams, intimate consumer electronic frame materials, and biodegradable medicinal materials [11–14].

However, there is a high complexity in the fluidity of materials during hot deformation. In the past, traditional constitutive models were often built to study the mechanical properties of magnesium alloys [15]. In order to predict the flow behavior given different degrees of deformation, JAMIN *et al.* [16] used Johnson-Cook and Zerilli-Armstrong constitutive model to predict the flow-stress behaviour of AZ31B alloy under the temperature from 200–350 degrees C and the strain rates from 0.001–0.1s<sup>-1</sup>. SAHOO and PANIGRAHI [17] calculated the activation energy to reveal the mechanism behind the hot deformation behavior of magnesium matrix materials based on the constitutive model of all material conditions. MOTALLEBI *et al.* [18] introduced and analyzed the constitutive equations for heat flow stress modeling and prediction, including the

phenomenological model of Johnson-Cook model and Fields-Backofen model. NEEHU *et al.* [19] adopted the Arrhenius model of strain compensation to investigate the hot deformation behavior of Mg-8Zn-4Y at the temperature of 523K–673K and the strain rate of  $0.001s^{-1} - 0.3s^{-1}$ . In fact, when the traditional constitutive equation is used to examine the properties of magnesium alloys, it is often disadvantaged by the inadequate accuracy of prediction and the inability to accurately reflect the hot deformation behavior of magnesium alloys at different strain rates.

The stress prediction model of magnesium alloy established using intelligent algorithms not only effectively assesses the mechanical properties of the alloy during the hot deformation process, but also exhibits enhanced flexibility and adaptability when compared to traditional methods. Therefore, the use of various novel intelligent algorithms to develop stress prediction models for magnesium alloy is increasingly gaining recognition. In the last two years, relevant researches have included: LIU *et al.* [20] predicted the hot deformation behaviour of Mg-2Nd alloy by utilizing the Arrhenius model and support vector regression (SVR) method, based on a hot compression test of Mg-2Nd alloy under the conditions of 150–300 degrees C and the strain rate of  $0.001-1s^{-1}$ . By comparing the prediction results, they found that the SVR model shows better accuracy in predicting rheological stress of Mg-2Nd alloy than the Arrhenius model. After that, for the sake of identifying the optimal processing window of Mg-3Dy alloy, LIU's *et al.* team [21] used the particle swarm optimization (PSO) algorithm to optimize SVR this time, then predicted the flow-stress of Mg-3Dy alloy under deformation parameters of 380–470 degrees C and the strain rates of  $0.001-1s^{-1}$ , the accuracy of PSO-SVR model was proved to be good. GAIROLA *et al.* [22] researched the hot deformation behaviour of AlSi10Mg alloy over a range of 150–300 degrees C,  $0.01-1s^{-1}$ , and predicted its flow-stress by a series of constitutive models and ANN. Among these models, ANN showed the highest accuracy. NING *et al.* [23] proposed an artificial neural network (ANN) model optimized by Northern Goshawk (NGO) algorithm to research the hot deformation rule of AZ42 alloy at a temperature scope of 250–400 degrees C and the strain rates of  $0.001-1s^{-1}$ . The results proved that the NGO-ANN model established has satisfactory accuracy, and NING's team obtained the optimal process domain where the mechanical properties of AZ42 alloy are best. In addition, the prediction of the hot deformation behavior of magnesium alloys is also very helpful for the development of new materials. For example, THAMARAI SELVAN and PALANI [24] tried to use ANN to predict the mechanical properties of AZ31 alloy with compositions of various metals like Al, Zn, Mn and Ca, with different proportions. Through this way, they wanted to find the best proportioning scheme to make the alloy suitable for orthopedic surgery, and can meet the mechanical properties and biocompatibility at the same time. Summary information on the application of ML methods in the related studies is listed in Table 1.

**Table 1:** Performance summary of published ML models used to predict the mechanical properties of magnesium alloy.

MODEL			DATA DESCRIPTION		PERFORMANCE
PREDICTION OBJECT	AUTHORS	TECHNIQUES	DATASET	INPUT VARIABLES	ERROR
Mg-2Nd alloy	Liu, <i>et al.</i> , (2024)	SVR	—	temperature, strain rate, strain of the alloy	$R^2 = 0.99975$ MSE = 0.9375
Mg-3Dy alloy	Liu, <i>et al.</i> , (2024)	PSO-SVR	1104 data points	temperature, strain rate, strain of the alloy	$R^2 = 0.99982$ MSE = 0.074
AlSi10Mg	Gairola <i>et al.</i> , (2024)	ANN	632 data points	temperature, strain rate, strain of the alloy	$R^2 = 0.999$ AARE = 0.5% RMSE = 2.51
Mg42 alloy	Ning <i>et al.</i> , (2023)	NGO-ANN	1010 data points	number of neurons, threshold of neurons, weight factor, population size, maximum iteration limit	$R^2 = 0.991$ MAPE = 3.51% RMSE = 2.73
AZ31	Thamarai and Palani, (2023)	ANN	—	number of neurons, threshold of neurons, weight factor, yield strength of alloy	$R^2 = 0.983$ RMSE = 6.73

The review of the relevant studies in the past few years can reveal that most of the studies on mechanical properties of magnesium alloy during hot deformation process prefer to use ANN technique, while no researchers have previously applied extreme learning machine (ELM) in this field. Compared with a single-layer ANN, ELM with a single hidden layer learning parameters (weights and thresholds) has a significant advantage that it does not need subsequent iterations to obtain the optimal value of it [25]. Therefore, a powerful ELM technique which optimizes ELM by tent chaotic map-sparrow search algorithm (TCMSSA) is introduced in this study. Among the novelties of the technique is that it tactfully avoids some shortcomings of traditional ELM like randomness in the selection of weights and thresholds [26], by combining optimization algorithms to enhance its prediction accuracy. In order to eliminate the weaknesses of ELM, in this study, an improved sparrow search algorithm (SSA) optimized by tent chaotic map (TCM) for the initial population is configured. This hybrid algorithm has stronger global optimization ability than traditional SSA and can optimize the selection of weights and thresholds of ELM to avoid it falling into local minimum and failing to reach global minimum in this work, thus improving its robustness. The prediction results show that the accuracy of the proposed method in this study (average value of RMSE = 1.0833, average value of  $R^2 = 0.99913$ ) is higher than that of ANN models, and compared with particle swarm optimization (PSO) and genetic algorithm (GA), TCMSSA algorithm is more suitable for optimizing ELM model, which greatly improves its prediction performance. The method in this study contributes a new optimization strategy to the prediction as to mechanical properties of AZ80 magnesium alloy in each molding stage.

## 2. SSA IMPROVEMENT PRINCIPLE AND ELM MODEL OPTIMIZATION

### 2.1. SSA principle

The SSA is a new intelligent optimization algorithm put forward by XUE and SHEN [27], and the mathematical model is established by analyzing the predatory and avoidance behaviors of the sparrow population.

To simulate the process of sparrows searching for food, the sparrow population is first initialized and defined as

$$X = \begin{pmatrix} x_1^1 & x_1^2 & \cdots & x_1^d \\ x_2^1 & x_2^2 & \cdots & x_2^d \\ \vdots & \vdots & \cdots & \vdots \\ x_n^1 & x_n^2 & \cdots & x_n^d \end{pmatrix} \quad (1)$$

in equation (1):

$n$  — the total number of sparrows in this population;

$d$  — the dimension of variables to be optimized;

$x_n^d$  — the value of dimension  $d$  of the  $n$ -th sparrow.

With the fitness of the first sparrow expressed as  $f([x_1^1 \ x_1^2 \ \cdots \ x_1^d])$ , that of the sparrow population is expressed as

$$F_x = \begin{pmatrix} f([x_1^1 \ x_1^2 \ \cdots \ x_1^d]) \\ f([x_2^1 \ x_2^2 \ \cdots \ x_2^d]) \\ \vdots \\ f([x_n^1 \ x_n^2 \ \cdots \ x_n^d]) \end{pmatrix} \quad (2)$$

in equation (2),  $f$  denotes the fitness. In the search process conducted by SSA, the sparrow individuals who find the food first have higher fitness. The followers indicate the direction of foraging under the guidance of the discoverers. Therefore, the scope of food search by the discoverers is wider compared to that of the followers.

During each iteration, there is change to the location information of the discoverers. The location update can be written as

$$X_{i,j}^{m+1} = \begin{cases} X_{i,j}^m \exp\left(-\frac{i}{\alpha \cdot iter_{max}}\right), & R < ST \\ X_{i,j}^m + QL, & R \geq ST \end{cases} \quad (3)$$

in equation (3):

$m$  — the number of current iterations;

$X_{i,j}^{m+1}$  — the value of the  $j$ -th dimension of the  $i$ -th sparrow in the  $m + 1$  iteration and  $j = 1, 2, 3, \dots, d$ ;

$\alpha$  —  $\alpha \in 0, 1$ , indicates a random number;

$iter_{max}$  — the maximum number of iterations;

$R$  —  $R \in 0, 1$ , refers to the warning value;

$ST$  —  $ST \in 0, 1$ , represents the safety value;

$Q$  — a random number subject to normal distribution;

$L$  — a matrix of  $1 \times d$ , where each element is 1.

when  $R < ST$ , the area where the sparrow is located is safe, and the finders can conduct an extensive search for food. When  $R \geq ST$ , some sparrows detect predators and issue an alert to other sparrows. Then, all the sparrows in the population fly to a safe area for feeding.

For the followers, once the discoverers find good food sources, they will know and fly to the nearby area for food. The equation for updating the location of followers can be expressed as

$$X_{i,j}^{m+1} = \begin{cases} Q \cdot \exp\left(\frac{X_{worst}^m - X_{i,j}^m}{i^2}\right), & i \leq n/2 \\ X_p^{m+1} + |X_{i,j}^m - X_p^{m+1}| \cdot A^+ \cdot L, & i > n/2 \end{cases} \quad (4)$$

in equation (4):

$X_p$  — the optimal position of the discoverers;

$X_{worst}$  — the worst position of the current population;

$A^+$  —  $A^+ = A^T(AA^T)^{-1}$ ,  $A$  refers to a matrix of  $1 \times d$ , where each element is randomly assigned to 1 or  $-1$ .

when  $i > n/2$ , the first follower with a low fitness has no access to food.

In the SSA, the location-updating equation of the watchers is defined as

$$X_{i,j}^{m+1} = \begin{cases} X_{best}^m + \beta \cdot |X_{i,j}^m - X_{best}^m|, & f_i > f_g \\ X_{i,j}^m + K \cdot \left(\frac{|X_{i,j}^m - X_{worst}^m|}{(f_i - f_w) + \varepsilon}\right), & f_i = f \end{cases} \quad (5)$$

in equation (5):

$X_{best}$  — the current global optimal position;

$\beta$  — a step control parameter, which is a random number subject to the standard normal distribution;

$K$  —  $K \in [-1, 1]$ , is a random number which represents the control factor of the movement direction and the step size;

$f_i$  — the fitness of current sparrow individual;

$f_g$  and  $f_w$  — the best fitness and the worst fitness;

$f_w$  — the worst fitness;

$\varepsilon$  — a small constant needed to avoid zero denominator.

## 2.2. TCM algorithm

Before the iteration of the basic SSA, the randomly generated sparrow population is subjected to the limitation of uneven regional distribution and relatively single population. Consequently, the search efficiency decreases in the iteration process. The TCM algorithm, as a piecewise linear two-dimensional chaotic mapping, offers advantages such as a uniform distribution function and strong correlation [28]. Herein, TCM is expressed as [29]

$$\begin{cases} H_{t+1} = \frac{H_t}{\eta} & 0 < H_t < \eta \\ H_{t+1} = \frac{(1-H_t)}{(1-\eta)} & \eta \leq H_t < 1 \end{cases} \quad (6)$$

in equation (6):

- $H_t$  — the chaotic mapping value at time  $t$ ;
- $\eta$  — the chaos coefficient.

within the value range of TCM parameters, the nonlinear system is in a chaotic state and it is characterized by uncertainty, uniqueness and unpredictability. Besides, the state of the sparrow population can not be repeated within a certain range.

As shown in Figure 1, the blue circle and the red triangle represent the initial values generated by the chaotic model and the random number, respectively. Although the random number has a set of values in the elliptical box, there is barely any value in the rectangular box. For this reason, TCM algorithm is adopted as replacement for the initialization of random number. In addition to maintaining the diversity and the coverage of the population, TCM algorithm also separates the algorithm from the local optimal value and improves the capability of global search [30]. In this work, chaos initialization model is applied to update the discoverers, the followers and the watchers.

### 2.3. Extreme learning machine

The ELM model was proposed by HUANG *et al.* [31], is a single hidden layer feed forward neural network algorithm that primarily utilizes the generalized inverse theory of matrices. ELM is one of the fastest neural

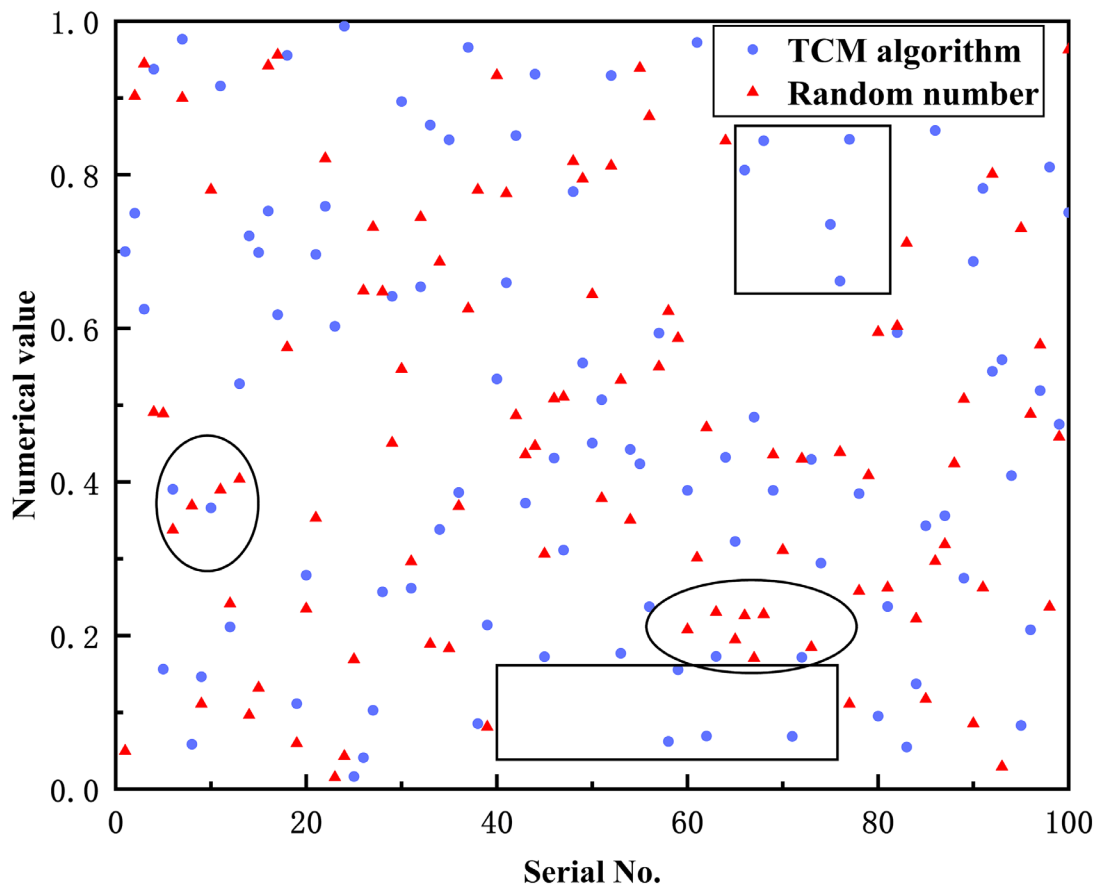
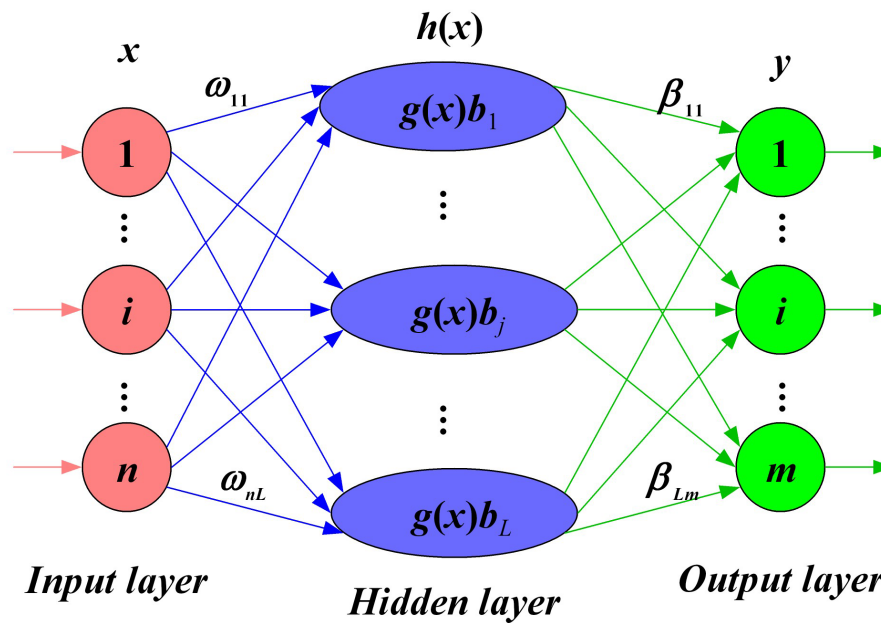


Figure 1: Initialized comparison between TCM algorithm and random number.

networks with less learning time, higher accuracy and stronger generalizability [32]. Since its introduction, it has been widely used to solve various problems such as classification, clustering and regression [33].

The fundamental structure of ELM consists of three layers, which are respectively input layer, hidden layer and output layer. Distinct from the BP neural network algorithm, ELM does not require iterative adjustments of connection weights  $\omega$  and thresholds  $b$  in the hidden and input layers. Since they can be set randomly, computational load of ELM can be reduced by half. Meanwhile, the connection weight between the output layer and the hidden one is needless to be updated through iteration, which further enhances the generalization performance of the model and significantly improves the optimization speed. Compared with other traditional algorithms, the ELM model shows such advantages as a better capability of function approximation and fewer setting parameters, which has attracted attention from many scholars for research [34–37]. The ELM neural network is illustrated in Figure 2.



**Figure 2:** ELM neural network.

in Figure 2:

- $x_1 \sim x_n$  — the node of input neuron;
- $\omega_{11} \sim \omega_{nk}$  — the weight between the input layer and the hidden one;
- $g(x)$  — the activation function;
- $b_1 \sim b_L$  — the hidden layer node threshold;
- $\beta_{11} \sim \beta_{nk}$  — the weight between the hidden layer and the output one;
- $y_1 \sim y_m$  — the output of the ELM neural network.

#### 2.4. TCMSSA-ELM model

The detailed optimization flowchart of TCMSSA-ELM model is illustrated in Figure 3. Despite ELM has considerable advantages, it still suffers a problem that cannot be ignored. When ELM model is utilized for predicting the mechanical properties of AZ80 magnesium alloy with a constant number of training sets, the primary factors impacting the prediction accuracy are the two parameters which are input layer connection weight  $\omega$  and the hidden layer threshold  $b$ . Typically, these parameters are randomly generated by the algorithm or manually debugged by the operator, so it is quite possible that they are not optimal during training, which may lead to issues such as reduced prediction accuracy, sluggish convergence, and the potential occurrence of “over fitting” [38, 39]. If a large number of hidden layer neurons are set in the training process for pursuing higher prediction accuracy, it often leads to many redundant neurons in the hidden layer, which will negatively affect the accuracy of the model on the contrary [25, 37].

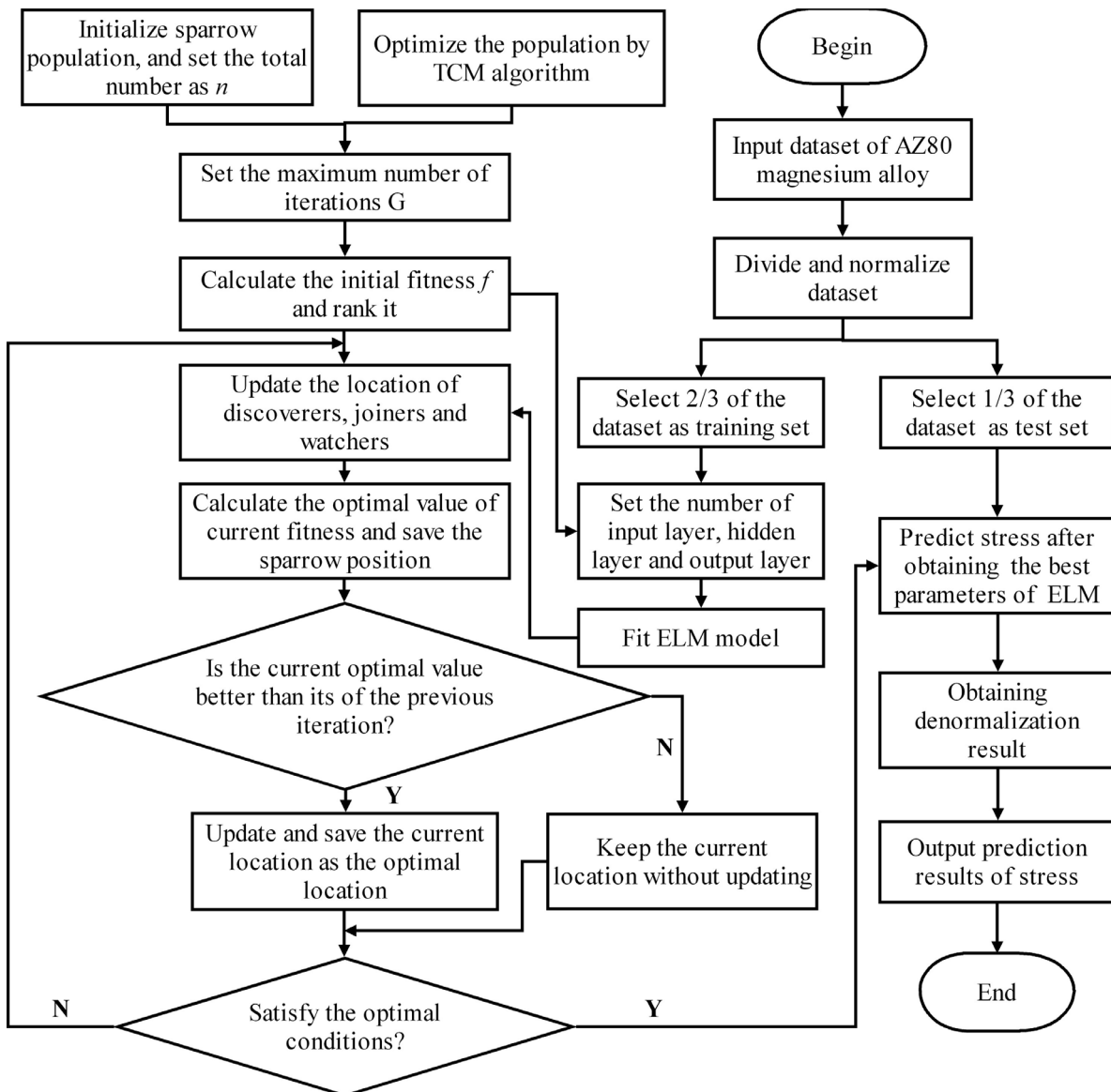


**Figure 3:** The optimization process of TCMSSA-ELM model.

In view of this, TCMSSA can be obtained from the SSA optimized by TCM algorithm, and it is applied to optimize the weights and thresholds of ELM, thus the TCMSSA-ELM model is constructed, which addresses the downsides of ELM in practical application. In the TCMSSA-ELM model, the input layer reflected by each sparrow in the population is used to connect the weight  $\omega$  and the hidden layer threshold  $b$ . Additionally, the TCM algorithm is introduced to update the positions of the discoverers, the joiners and the watchers in the sparrow population. In this way, the population ergodicity of sparrows is improved.

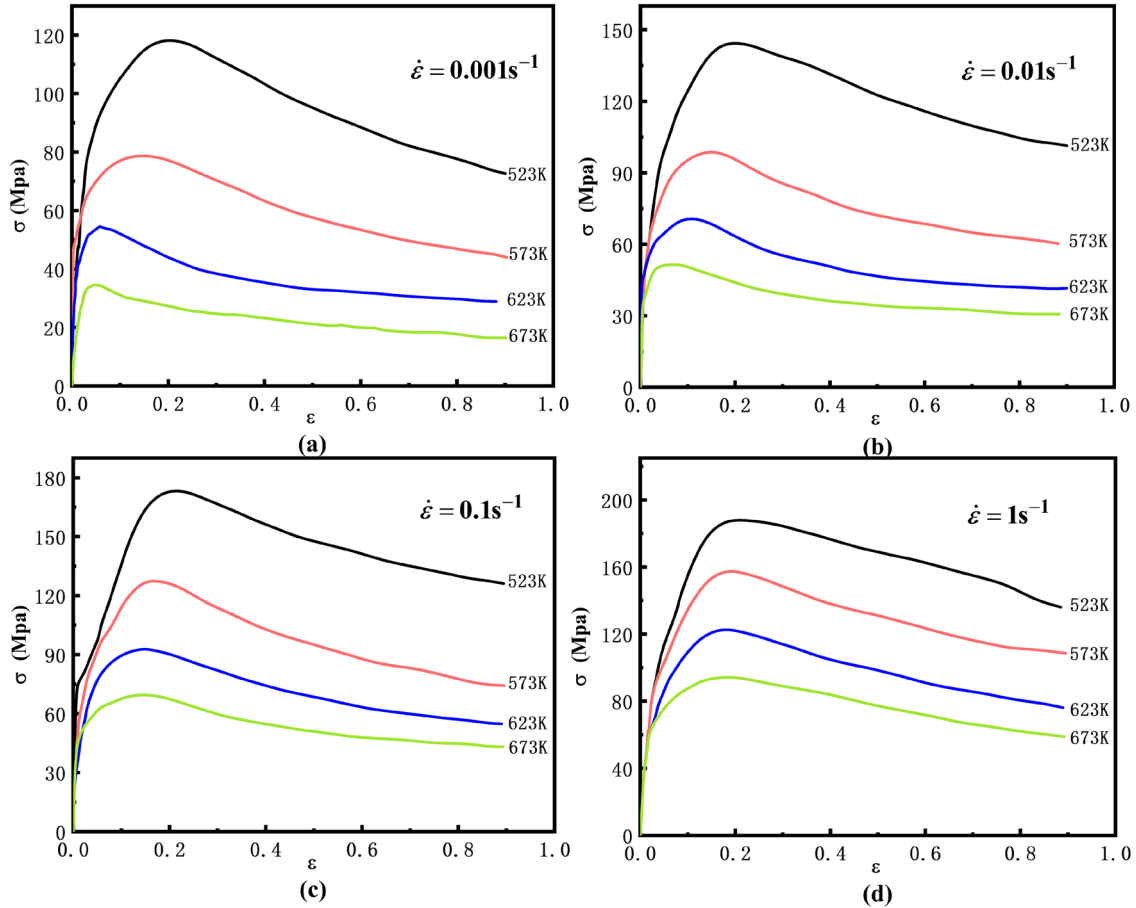
### 3. APPLICATION AND ACCURACY EVALUATION OF TCMSSA-ELM MODEL

#### 3.1. Stress strain data

The mechanical properties of AZ80 magnesium alloy are predicted in this work, and its chemical composition is listed in Table 2. Figure 4 shows the true stress-strain test curves of AZ80 magnesium alloy in literature [40] at different strain rates. There are 812 points on the stress-strain curves selected from 16 stress curves of Figure 4. The points on the 16 stress curves are divided into 16 groups. There are four lines under each strain rate, and at a specific strain rate, 2/3 of each group is used as the training set, and the others are taken as the test set.

**Table 2:** Chemical composition of AZ80 magnesium alloy (wt%).

Al	Zn	Mn	Si	Fe	Ni	Cu	Mg
8.360	0.524	0.385	0.076	0.005	0.006	0.003	Bal.

**Figure 4:** True stress-strain curves of AZ80 magnesium alloy at different stress rates: (a)  $\dot{\epsilon} = 0.001s^{-1}$ , (b)  $\dot{\epsilon} = 0.01s^{-1}$ , (c)  $\dot{\epsilon} = 0.1s^{-1}$  and (d)  $\dot{\epsilon} = 1s^{-1}$ .

### 3.2. Optimization algorithms for comparison

PSO and GA are reliable optimization techniques commonly used in various studies. In order to demonstrate the superiority of the proposed TCMSSA-ELM model in predicting the mechanical properties of magnesium alloys, PSO and GA are also employed to optimize ELM respectively, and the prediction results of ELM, PSO-ELM, GA-ELM and TCMSSA-ELM based on the same training dataset are compared.

PSO is a population-based stochastic optimization technique, initially introduced by Kennedy and Eberhart in 1995. In PSO algorithm, particles in the population, representing the potential solutions, have their own position and velocity characteristics, they collaboratively and iteratively explore the search space. During this process, two key attributes, the local best position and the global best position, guide the adjustment of each particle's position and evaluate its velocity, then particles gradually gather toward the best-known positions of the population in search of an optimal solution to the given problem [41]. Generally, PSO has the advantages of simplicity, it is often used to solve some complex optimization problems with fast convergence. However, it also has some defects such as it is easy to fall into local optimal and suffer premature convergence when dealing with large-scale problems [42].

GA is an evolutionary algorithm with satisfactory robustness and easily application. It can identify high performance solutions in each of its iterations and this will help find better solutions for the next iteration. Compared with other classic optimization algorithms, GA is known for its superior parallel processing capabilities. Nevertheless, poor adaptability has always been the main problem of it [43].



### 3.3. Model parameter setting

In order to assess the effectiveness and accuracy of the TCMSSA-ELM prediction model, the data from training set shown in Figure 4 are inputted into the model for training according to the process illustrated in Figure 3. After repeated calculations, it is concluded that 55 is the number of hidden layers, that leading to the minimum training error of the ELM model. The number of training times is set to 3000, the target error is set to 0.0001, and the initial population size is 20. In the sparrow population, 70% are discoverers, 20% are watchers with an alert value of 0.6, and the others are joiners. The control parameters of the established TCMSSA-ELM model are presented in Table 3 and that of the PSO-ELM and GA-ELM models used for comparison are listed in Table 4.

### 3.4. Stress prediction and comparative analysis of magnesium alloys

After stress prediction under different strain rates, the mean absolute percentage error (MAPE) is treated as the index of prediction accuracy evaluation for these models. It is often used to evaluate the errors between the predicted values and the actual ones, the smaller the value of MAPE (general requirement is less than 10%), the more accurate the prediction model. The calculation formula of MAPE is shown below:

$$MAPE = \frac{1}{N} \sum_{i=1}^N \left[ \left| \frac{y_{tested_i} - y_{predicted_i}}{y_{tested_i}} \right| \times 100\% \right] \quad (7)$$

**Table 3:** The control parameters of TCMSSA-ELM.

TCM		SSA		ELM	
CONTROL PARAMETERS	VALUE	CONTROL PARAMETERS	VALUE	CONTROL PARAMETERS	VALUE
Initial point	0.7	Max number of iterations	3000	Number of hidden layers	55
Max number of iterations	3000	Initial population	20	Transfer function	Sigmoidal function
		Proportion of discoverers	0.7	Type	Regression
		Proportion of watchers	0.2		
		Alert value	0.6		
		Proportion of joiners	0.1		

**Table 4:** The control parameters of PSO-ELM and GA-ELM.

PSO		GA		ELM	
CONTROL PARAMETER	VALUE	CONTROL PARAMETER	VALUE	CONTROL PARAMETER	VALUE
Maximum number of iterations	3000	Maximum number of iterations	3000	Number of hidden layers	55
Swarm size	20	Population	20	Transfer function	Sigmoidal function
Accelerated constant 1	2	Mutation rate	0.01	Type	Regression
Accelerated constant 2	2	Crossover rate	0.99		
Weight	0.8				
Max velocity	1				
Min velocity	-1				
Var Max	5				
Var Min	-5				

in equation (7):

$N$  — the number of samples;

$y_{tested_i}$  — the stresses of AZ80 obtained from the experiment;

$y_{predicted_i}$  — the stresses of AZ80 predicted.

The average MAPE values of four prediction models at all strain rates are listed in Table 5, and the corresponding MAPE curves at different strain rates are plotted in Figure 5. It can be seen clearly that all four models show high accuracy in predicting the mechanical properties of magnesium alloys, with MAPEs less than 10%. Among them, the original ELM demonstrates the worst accuracy and is far inferior to the other three optimized ELM models, the average MAPEs of GA-ELM, PSO-ELM and TCMSSA-ELM models are respectively 72.12%, 64.92% and 87.04% lower than that of ELM model (as shown in Table 5), this proves that the three optimization algorithms used in this study are indeed effective in improving the performance of ELM.

In addition, it is also obvious that the predictive performance of the four models is ranked as: TCMSSA-ELM > GA-ELM > PSO-ELM > ELM, and TCMSSA-ELM model apparently has the most advantages in predicting the mechanical properties of AZ80 magnesium alloy over PSO-ELM and GA-ELM due to the lowest MAPE values, which proves that TCMSSA algorithm has stronger ability to optimize ELM's weights and thresholds compared with PSO and GA algorithms.

Subsequently, in order to show the optimization amplitude of TCMSSA algorithm for ELM more intuitively, ELM and TCMSSA-ELM models are respectively used to predict the test set of stress  $\sigma$  of AZ80 magnesium alloy at each strain rate and the fitting curves based on ELM and TCMSSA-ELM models are drawn, as shown in Figure 6. To facilitate comparative analysis, the experimental values of the test set are also

**Table 5:** Average MAPEs of four prediction models at all strain rates.

	ELM	PSO-ELM	GA-ELM	TCMSSA-ELM
<b>AVERAGE MAPE</b>	5.9317%	2.0448%	1.8506%	1.0367%
<b>COMPARED WITH ELM</b>	—	↓ 64.92%	↓ 72.12%	↓ 87.04%

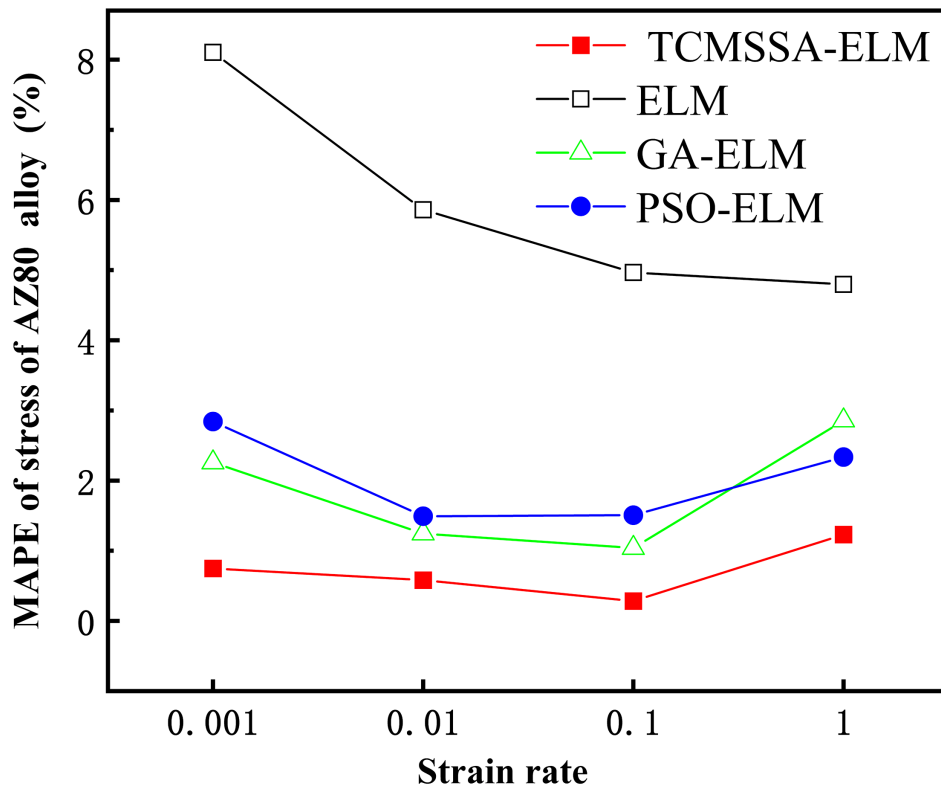


**Figure 5:** MAPEs of four prediction models at different strain rates.

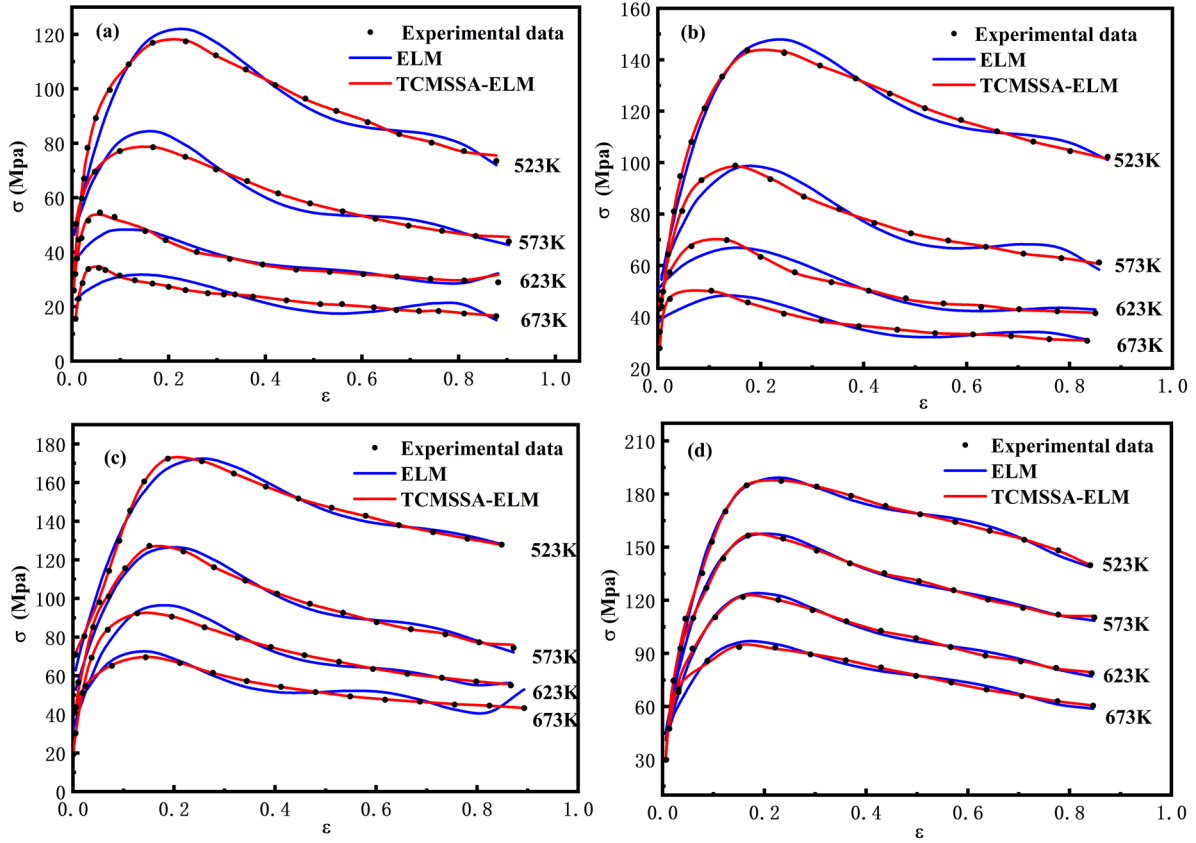


**Figure 6:** Predicted curves of two models (a)  $\dot{\epsilon} = 0.001s^{-1}$ , (b)  $\dot{\epsilon} = 0.01s^{-1}$ , (c)  $\dot{\epsilon} = 0.1s^{-1}$  and (d)  $\dot{\epsilon} = 1s^{-1}$ .

visualized in Figure 6. It is not difficult to find that although the fitting curves of ELM can generally conform to the variation rule of the experimental values, the prediction accuracy is still insufficient especially at low strain rates like and  $\dot{\epsilon} = 0.001s^{-1}$  and  $\dot{\epsilon} = 0.01s^{-1}$ , the deviation between fitting curves and the experimental values is very noticeable. Different from original ELM, regardless of the temperatures and the strain rates, the fitting curves of TCMSSA-ELM prediction model can reflect the varying trend in the true stress of magnesium alloy with strain precisely, which is manifested in that the experimental points basically fall onto the fitting curves of TCMSSA-ELM.

Take the experimental value as the abscissa one and the predicted value of ELM model as the ordinate one at different strain rates, as well as TCMSSA-ELM model, and the resulting points are plotted in Figure 7 and compared with the ideal 45° line. Apparently, ELM has a higher degree of data point dispersion, and the dispersion gradually increases with the decrease of strain rates. In contrast, the points from TCMSSA-ELM model better approach to the ideal 45° line at each strain rate.

Then analyzing the prediction results from the Angle of numerical differences, the coefficient of determination  $R^2$  is chosen as one of the evaluation indicators because it is often used to evaluate the goodness of fit of regression models,. the closer the value of  $R^2$  is to 1, the higher the goodness of fit, the evaluation results can be displayed more intuitively. Another indicator is the root mean square error (RMSE), it is sensitive to data outliers and easy to calculate. The relevant equations are expressed below:

$$R^2 = 1 - \frac{\sum_{i=1}^N (y_{predicted_i} - y_{tested_i})^2}{\sum_{i=1}^N \left( y_{predicted_i} - \frac{\sum_{i=1}^N y_{tested_i}}{N} \right)^2} \quad (8)$$

$$RMSE = \sqrt{\frac{1}{N} \sum_{i=1}^N (y_{tested_i} - y_{predicted_i})^2} \quad (9)$$

in equation (8) and (9), the meaning of parameters is consistent with that of equation (7). According to the calculation results, the values of  $R^2$  and RMSE of ELM and TCMSSA-ELM at different strain rates are listed in Table 6 and drawn as Figure 8 for easy comparison.

By observing Figure 8, it can be found that TCMSSA-ELM's values of  $R^2$  at all strain rates are extremely close to 1, indicating that the model's goodness of fit is satisfactory, while ELM is obviously inferior to TCMSSA-ELM especially under the condition of low strain rate. In the comparison of RMSE, the two models exhibit a more striking gap. Based on the rule that the smaller the RMSE, the higher the model accuracy, apparently the RMSE-values of TCMSSA-ELM are merely 1/4 or 1/3 of that of ELM at most strain rates, and the difference between the two is not that significant only when  $\dot{\epsilon} = 1s^{-1}$ . According to Table 6, the average

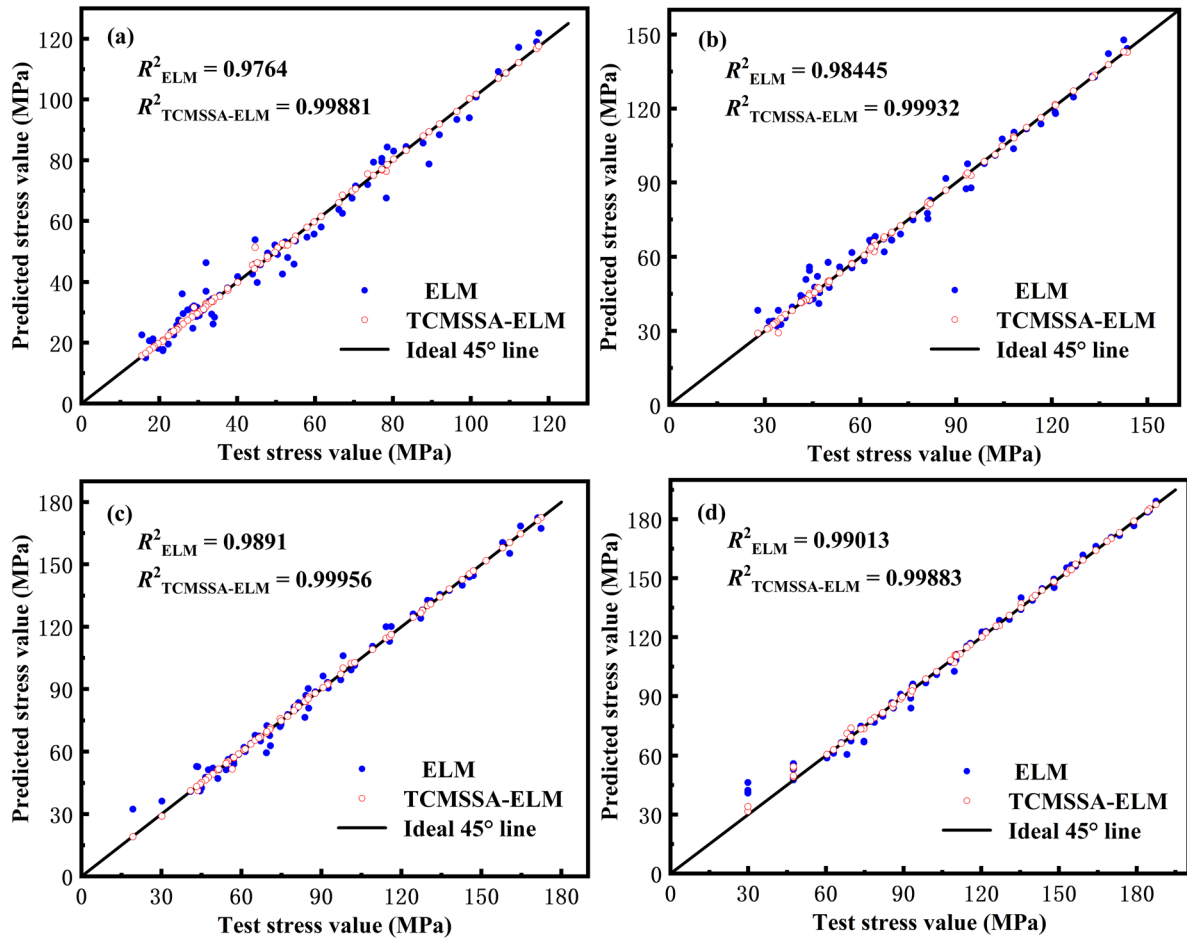


**Figure 7.** Correlation between predicted values and experimental ones (a)  $\dot{\epsilon} = 0.001s^{-1}$ , (b)  $\dot{\epsilon} = 0.01s^{-1}$ , (c)  $\dot{\epsilon} = 0.1s^{-1}$  and (d)  $\dot{\epsilon} = 1s^{-1}$ .

**Table 6:**  $R^2$  and RMSE of ELM and TCMSSA-ELM at different strain rates.

	STRAIN RATES $\dot{\epsilon}$				AVERAGE VALUE
	$0.001s^{-1}$	$0.01s^{-1}$	$0.1s^{-1}$	$1s^{-1}$	
$R^2_{ELM}$	0.9764	0.98445	0.9891	0.99013	0.98502
$R^2_{TCMSSA-ELM}$	0.99881	0.99932	0.99956	0.99883	0.99913
$RMSE_{ELM}$	4.2865	2.9037	2.2261	1.9743	2.8477
$RMSE_{TCMSSA-ELM}$	0.9936	0.8603	0.8139	1.6653	1.0833

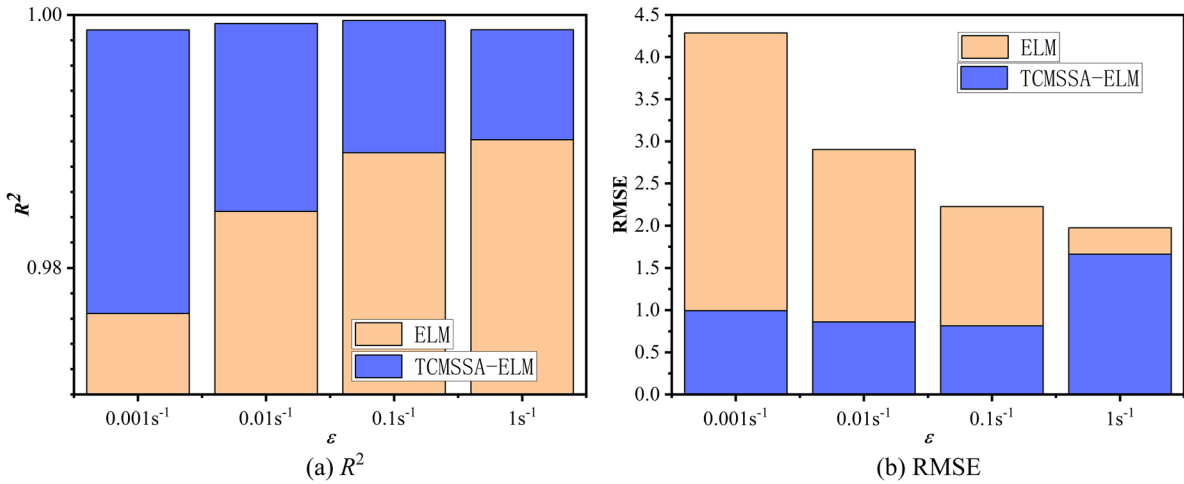


Figure 8. Comparisons between ELM and TCMSSA-ELM in R<sup>2</sup> and RMSE at different strain rates.

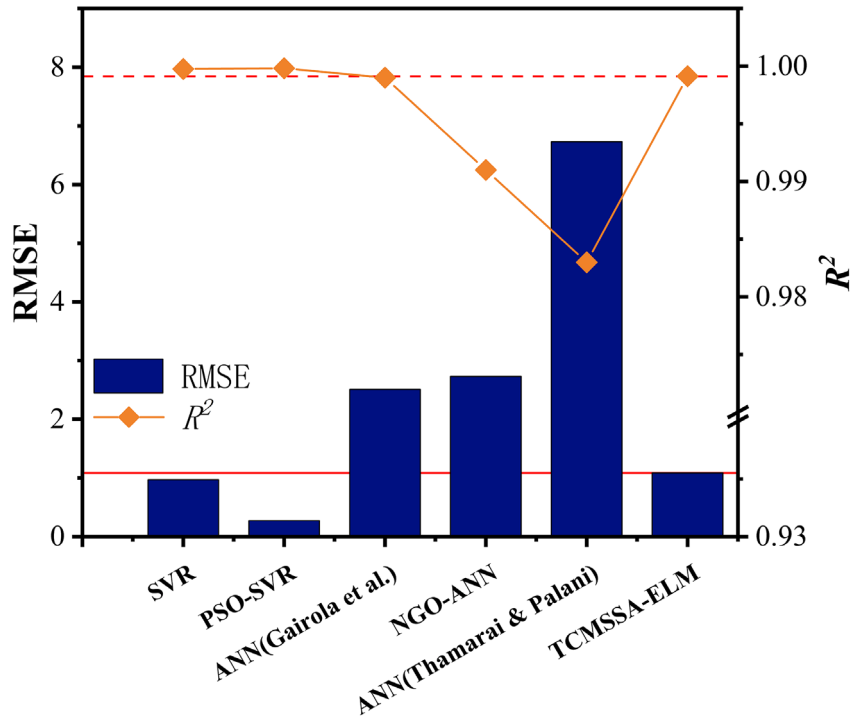


Figure 9. Comparison between TCMSSA and other related research methods in recent years.

value of  $R^2_{TCMSSA-ELM}$  is 0.99913, which is 1.43% higher than that of  $R^2_{ELM}$ . At the same time, the average value of RMSE of TCMSSA-ELM model is 1.0833, which is 61.96% lower in comparison to that of ELM model. All of these comparison results from Table 6 and Figure 8 can once again suggest an evident improvement of ELM's performance based on the optimization of TCMSSA algorithm.

Finally, TCMSSA-ELM model proposed in this study is compared with the methods used in other relevant studies in the past two years [20–24], values of R<sup>2</sup> and RMSE are still used as evaluation indicators (some studies only provided MSE values, so let:  $RMSE = \sqrt{MSE}$ ), and the comparison results are plotted in Figure 9. As can be seen from Figure 9, performance of TCMSSA-ELM on magnesium alloy's stress prediction is significant stronger than that of ANN, and almost equivalent to SVR models. Considering that ELM has the advantage of faster processing speed with data, TCMSSA-ELM model is very competitive in the field of magnesium alloy property prediction.

#### 4. LIMITATIONS AND FUTURE RESEARCH PROSPECTS

This study highlights the practical value of TCMSSA-ELM model. However, the method proposed indeed has some limitations as follows:

1. The trained TCMSSA-ELM model can only predict the stress change during the process of magnesium alloy hot deformation temporarily.
2. Due to limited resources, there exists temporary difficulties to validate whether TCMSSA-ELM model is also applicable to different magnesium alloys through other datasets.

Therefore, future studies are required to consider collecting more hot compression test datasets covering various kinds of magnesium alloys to further verify whether TCMSSA-ELM is equally applicable to all magnesium alloys. This will become the top priority of future work. Moreover, future studies may also include the exploration of TCMSSA-ELM's application in predicting other properties of magnesium alloys, such as corrosion resistance and wear properties, as well as the research of some new magnesium alloys by adjusting the original material ratios with the help of the intelligent algorithm prediction model established in this study and necessary experiments.

#### 5. CONCLUSIONS

In this work, TCMSSA model was used for the mechanical property prediction of AZ80 magnesium alloy during hot deformation process based on a hot compression test with temperature range of 523K – 673K and strain rate range of  $0.001s^{-1}$ – $1s^{-1}$ . To create ML modes, 2/3 of the dataset was set as a training set and the rest as a test set.

TCMSSA model established in this study is a novel ML algorithm that has distinct advantages over the other artificial neural network algorithms. First, it has some positive characteristics like good performance, high accuracy and simple algorithm learning derived from ELM algorithm. Moreover, by utilizing TCMSSA algorithm to optimize ELM, some original defects of ELM such as randomness in the selection of weights and thresholds are eliminated, which further strengthens the robustness of ELM. These advantages distinguish TCMSSA model from other ML models.

In order to verify the superiority of TCMSSA, the prediction results are compared with those of ELM, GA-ELM and PSO-ELM models. The main conclusions are as follows:

1. The prediction accuracy of ELM model is not satisfactory especially under the condition of low strain rates, and the lower the strain rate, the lower the prediction accuracy of ELM.
2. TCMSSA-ELM model exhibits a high precision in predicting the mechanical properties of AZ80 magnesium alloy, with a low average value of MAPE of 1.0367% and RMSE of 1.0833. Average value of  $R^2$  is 0.99913, which is very close to 1. In terms of numerical errors, the prediction performance of TCMSSA-ELM is better than that of ANN models.
3. For the prediction of flow stress of AZ80 magnesium alloy at various temperatures and strain rates, the errors of ELM, PSO-ELM, GA-ELM and TCMSSA-ELM models decrease in sequence. Compared with the MAPE 5.9317% of ELM model used to predict the magnesium alloy stress, those of PSO-ELM and GA-ELM models are 2.0448% and 1.8506%, respectively, reducing by 72.12% and 64.92%, while that of TCMSSA-ELM model is only 1.0367%, reducing by 87.04%, indicating that TCMSSA algorithm presents better model optimization performance than PSO and GA algorithms.
4. The average value of  $R^2$  and RMSE of TCMSSA-ELM are respectively increased by 1.43% and decreased by 61.96% in contrast to ELM model, as well as the data points formed by predicted values and experimental ones are closer to the ideal 45° line. These means that TCMSSA algorithm indeed helps ELM improve its prediction performance, and better reflect the relationship between stress and strain of AZ80 magnesium alloy at each strain rate and temperature ultimately.

The above conclusions are sufficient to prove that TCMSSA model has good feasibility in predicting the mechanical properties of magnesium alloys.

## 6. ACKNOWLEDGMENTS

This work is sponsored by National Natural Science Foundation of China (12172228, 11572187), Natural Science Foundation of Shanghai (22ZR1444400), the Program of Foundation of Science and Technology Commission of Shanghai Municipality (22dz1206005, 22dz1204202) and Shanghai Professional Technical Service Platform for Intelligent Operation and Maintenance of Renewable Energy (22DZ2291800).

## 7. BIBLIOGRAPHY

- [1] WANG, K., WANG, X., WANG, J., *et al.*, “The development of a high-strength Mg-10.3Gd-4.4Y-0.9Zn-0.7Mn alloy subjected to large differential-thermal extrusion and isothermal aging”, *Materials (Basel)*, v. 16, n. 18, pp. 6103, Sep. 2023. doi: <http://doi.org/10.3390/ma16186103>. PubMed PMID: 37763381.
- [2] CAI, Z.-H., JIA, Y.-Y., HOU, Y.-J., *et al.*, “A High strength-ductility balanced Mg-1Ca-0.5Mn-0.53Ce Mg alloy sheet by multi-pass low-temperature rolling”, *Journal of Materials Engineering and Performance*, v. 33, n. 1, pp. 330–335, Jan. 2024. doi: <http://doi.org/10.1007/s11665-023-07952-z>.
- [3] GAO, M., CEN, L., JIANG, L., *et al.*, “Oscillating laser-arc hybrid additive manufacturing of AZ31 magnesium alloy”, *Applied Sciences (Basel, Switzerland)*, v. 13, n. 2, pp. 897, 2023. doi: <http://doi.org/10.3390/app13020897>.
- [4] DUTTA, S., MANDAL, S., GUPTA, S., *et al.*, “Effects of cerium addition on the corrosion resistance and biocompatibility of Mg-2Sr-1Zr alloy”, *Journal of Materials Research*, v. 35, n. 22, pp. 3124–3135, Nov. 2020. doi: <http://doi.org/10.1557/jmr.2020.255>.
- [5] ZHANG, C., LIANG, C., LIANG, T., *et al.*, “Enhanced mechanical properties of an Mg-Zn-Ca alloy via high pressure torsion and annealing for use in bone implantation”, *Matéria (Rio de Janeiro)*, v. 27, n. 3, pp. e20220005, 2022. doi: <http://doi.org/10.1590/1517-7076-rmat-2022-0005>.
- [6] REZANEZHAD, S., AZADI, M., “Amazing epsilon-shaped trend for fretting fatigue characteristics in AM60 magnesium alloy under stress-controlled cyclic conditions at bending loads with zero mean stress”, *PLoS One*, v. 18, n. 2, Feb. 2023. doi: <http://doi.org/10.1371/journal.pone.0281263>. PubMed PMID: 36749773.
- [7] KASHYZADEH, K.R., PAHLAVANI, M., MARZBANRAD, J., “High-temperature tensile behavior and high-cycle fatigue properties of Mg-7Li-1Zn alloy”, In: *Innovative Manufacturing, Mechatronics and Materials Forum (iM3F)*, Univ Malaysia Pahang, 2021. doi: <http://doi.org/10.1016/j.matpr.2020.07.370>.
- [8] CHENG, C., LI, X., LE, Q., *et al.*, “Effect of REs (Y, Nd) addition on high temperature oxidation kinetics, oxide layer characteristic and activation energy of AZ80 alloy”, *Journal of Magnesium and Alloys*, v. 8, n. 4, pp. 1281–1295, Dec. 2020. doi: <http://doi.org/10.1016/j.jma.2019.09.013>.
- [9] NIKNEJAD, S., LIU, L., LEE, M., *et al.*, “Resistance spot welding of AZ series magnesium alloys: Effects of aluminum content on microstructure and mechanical properties”, *Materials Science and Engineering a-Structural Materials Properties Microstructure and Processing*, v. 618, pp. 323–334, 2014.
- [10] PRAKASH, P., WELLS, M.A., WILLIAMS, B.W., “Hot deformation of cast AZ31 and AZ80 magnesium alloys – Influence of Al content on microstructure and texture development”, *Journal of Alloys and Compounds*, v. 897, pp. 162876, Mar. 2022. doi: <http://doi.org/10.1016/j.jallcom.2021.162876>.
- [11] LIU, L., WANG, N., LIU, Y., *et al.*, “Microstructure evolution and mechanical anisotropy of AZ80-Ag magnesium alloy: effect of isothermal semi-closed die forging and subsequent aging”, *Materials Science and Engineering A*, v. 862, pp. 144494, 2023. doi: <http://doi.org/10.1016/j.msea.2022.144494>.
- [12] HE, H., HUANG, S., YI, Y., *et al.*, “Simulation and experimental research on isothermal forging with semi-closed die and multi-stage-change speed of large AZ80 magnesium alloy support beam”, *Journal of Materials Processing Technology*, v. 246, pp. 198–204, Aug. 2017. doi: <http://doi.org/10.1016/j.jmatprotec.2017.03.015>.
- [13] ZHAO, N., WATSON, N., XU, Z., *et al.*, “In vitro biocompatibility and endothelialization of novel magnesium-rare earth alloys for improved stent applications”, *PLoS One*, v. 9, n. 6, Jun. 2014. doi: <http://doi.org/10.1371/journal.pone.0098674>. PubMed PMID: 24921251.
- [14] HE, L., YANG, J., XIONG, Y., *et al.*, “Effect of solution pH on stress corrosion cracking behavior of modified AZ80 magnesium alloy in simulated body fluid”, *Materials Chemistry and Physics*, v. 261, pp. 124232, Mar. 2021. doi: <http://doi.org/10.1016/j.matchemphys.2021.124232>.

- [15] XIAO, P., GAO, Y., XU, F., *et al.*, “Hot deformation behavior of in-situ nanosized TiB<sub>2</sub> particulate reinforced AZ91 Mg matrix composite”, *Journal of Alloys and Compounds*, v. 798, pp. 1–11, Aug. 2019. doi: <http://doi.org/10.1016/j.jallcom.2019.05.244>.
- [16] JAIMIN, A., MAHALLE, G., KOTKUNDE, N., *et al.*, “Integrated Johnson-Cook and Zerilli-Armstrong constitutive model for flow-stress prediction of AZ31B alloy”, *Advances in Materials and Processing Technologies*, 2023. doi: <http://doi.org/10.1080/2374068X.2023.2199476>.
- [17] SAHOO, B.N., PANIGRAHI, S.K., “Deformation behavior and processing map development of AZ91 Mg alloy with and without addition of hybrid in-situ TiC+TiB<sub>2</sub> reinforcement”, *Journal of Alloys and Compounds*, v. 776, pp. 865–882, Mar. 2019. doi: <http://doi.org/10.1016/j.jallcom.2018.10.276>.
- [18] MOTALLEBI, R., SAVAEDI, Z., MIRZADEH, H., “Additive manufacturing: a review of hot deformation behavior and constitutive modeling of flow stress”, *Current Opinion in Solid State and Materials Science*, v. 26, n. 3, pp. 100992, Jun. 2022. doi: <http://doi.org/10.1016/j.cossms.2022.100992>.
- [19] NEETHU, N., HASSAN, N.A., KUMAR, R.R., *et al.*, “Comparison of prediction models for the hot deformation behavior of cast Mg-Zn-Y alloy”, *Transactions of the Indian Institute of Metals*, v. 73, n. 6, pp. 1619–1628, Jun. 2020. doi: <http://doi.org/10.1007/s12666-020-01944-6>.
- [20] LIU, Y., YANG, T., LIU, Q., *et al.*, “Thermal deformation behavior of as-cast Mg-2Nd alloy: constitutive equation, microstructural analysis, and rheological stress prediction based on support vector regression”, *Journal of Materials Science*, v. 59, n. 19, pp. 8492–8514, May. 2024. doi: <http://doi.org/10.1007/s10853-024-09669-3>.
- [21] LIU, Y., FENG, Y., LIU, Q., *et al.*, “Prediction of flow stress in Mg-3Dy alloy based on constitutive equation and PSO-SVR model”, *Materials Research Express*, v. 11, n. 5, pp. 056513, May. 2024. doi: <http://doi.org/10.1088/2053-1591/ad48de>.
- [22] GAIROLA, S., SINGH, G., JAYAGANTHAN, R., “On the prediction of flow stress behavior of additively manufactured alsil0mg for high temperature applications”, *Journal of Materials Engineering and Performance*, 2024. doi: <http://doi.org/10.1007/s11665-024-09553-w>.
- [23] NING, M., CHEN, X., LIN, Y., *et al.*, “Revealing the hot deformation behavior of AZ42 Mg alloy by using 3D hot processing map based on a novel NGO-ANN model”, *Journal of Materials Research and Technology*, v. 27, pp. 2292–2310, 2023. doi: <http://doi.org/10.1016/j.jmrt.2023.10.073>.
- [24] THAMARAI SELVAN, A., PALANI, S., “Prediction of mechanical strength of magnesium alloy AZ31 with calcium addition using a neural network based model”, *Journal of Physics: Conference Series*, v. 2484, n. 1, pp. 012015, 2023. doi: <http://doi.org/10.1088/1742-6596/2484/1/012015>.
- [25] ABAD, A.R.B., MOUSAVI, S., MOHAMADIAN, N., *et al.*, “Hybrid machine learning algorithms to predict condensate viscosity in the near wellbore regions of gas condensate reservoirs”, *Journal of Natural Gas Science and Engineering*, v. 95, pp. 104210, Nov. 2021.
- [26] RAJABI, M., BEHESHTIAN, S., DAVOODI, S., *et al.*, “Novel hybrid machine learning optimizer algorithms to prediction of fracture density by petrophysical data”, *Journal of Petroleum Exploration and Production Technology*, v. 11, n. 12, pp. 4375–4397, Dec. 2021. doi: <http://doi.org/10.1007/s13202-021-01321-z>.
- [27] XUE, J., SHEN, B., “A novel swarm intelligence optimization approach: sparrow search algorithm”, *Systems Science & Control Engineering*, v. 8, n. 1, pp. 22–34, Jan. 2020. doi: <http://doi.org/10.1080/21642583.2019.1708830>.
- [28] LI, Y., HAN, M., GUO, Q., “Modified whale optimization algorithm based on tent chaotic mapping and its application in structural optimization”, *KSCE Journal of Civil Engineering*, v. 24, n. 12, pp. 3703–3713, Dec. 2020. doi: <http://doi.org/10.1007/s12205-020-0504-5>.
- [29] SHUXIAN, D., CHUNGUANG, B., YONGLIANG, W., “Improved whale optimization algorithm based on the tent chaotic mapping and nonlinear convergence factor”, *Journal of Physics: Conference Series*, v. 1682, n. 1, pp. 012055, 2020. doi: <http://doi.org/10.1088/1742-6596/1682/1/012055>.
- [30] PAKNEJAD, P., KHORSAND, R., RAMEZANPOUR, M., “Chaotic improved PICEA-g-based multi-objective optimization for workflow scheduling in cloud environment”, *Future Generation Computer Systems*, v. 117, pp. 12–28, Apr. 2021. doi: <http://doi.org/10.1016/j.future.2020.11.002>.
- [31] HUANG, G.-B., WANG, D.H., LAN, Y., “Extreme learning machines: a survey”, *International Journal of Machine Learning and Cybernetics*, v. 2, n. 2, pp. 107–122, Jun. 2011. doi: <http://doi.org/10.1007/s13042-011-0019-y>.



- [32] RAJABI, M., GHORBANI, H., AGHDAM, K., “Prediction of shear wave velocity by extreme learning machine technique from well log data”, *Journal of Petroleum Geomechanics*, v. 4, n. 3, pp. 35–49, 2022.
- [33] ABAD, A.R.B., GHORBANI, H., MOHAMADIAN, N., *et al.*, “Robust hybrid machine learning algorithms for gas flow rates prediction through wellhead chokes in gas condensate fields”, *Fuel*, v. 308, pp. 121872, Jan. 2022. doi: <http://doi.org/10.1016/j.fuel.2021.121872>.
- [34] SHEN, Y., WANG, P., WANG, X., *et al.*, “Application of empirical mode decomposition and extreme learning machine algorithms on prediction of the surface vibration signal”, *Energies*, v. 14, n. 22, pp. 7519, Nov. 2021. doi: <http://doi.org/10.3390/en14227519>.
- [35] LIU, Y., WANG, J., “Transfer learning based multi-layer extreme learning machine for probabilistic wind power forecasting”, *Applied Energy*, v. 312, pp. 118729, Apr. 2022. doi: <http://doi.org/10.1016/j.apenergy.2022.118729>.
- [36] JAMEI, M., HASANIPANAH, M., KARBASI, M., *et al.*, “Prediction of flyrock induced by mine blasting using a novel kernel-based extreme learning machine”, *Journal of Rock Mechanics and Geotechnical Engineering*, v. 13, n. 6, pp. 1438–1451, Dec. 2021. doi: <http://doi.org/10.1016/j.jrmge.2021.07.007>.
- [37] DAVOODI, S., MEHRAD, M., WOOD, D.A., *et al.*, “Hybridized machine-learning for prompt prediction of rheology and filtration properties of water-based drilling fluids”, *Engineering Applications of Artificial Intelligence*, v. 123, pp. 106459, Aug. 2023. doi: <http://doi.org/10.1016/j.engappai.2023.106459>.
- [38] WANG, X., WANG, C., LI, Q., “Short-term wind power prediction using GA-ELM”, *The Open Electrical & Electronic Engineering Journal*, v. 11, n. 1, pp. 48–56, 2017. doi: <http://doi.org/10.2174/1874129001711010048>.
- [39] WU, C., WANG, J., CHEN, X., *et al.*, “A novel hybrid system based on multi-objective optimization for wind speed forecasting”, *Renewable Energy*, v. 146, pp. 149–165, Feb. 2020. doi: <http://doi.org/10.1016/j.renene.2019.04.157>.
- [40] LI, Q., JIN, Z., “Comparative study of physical-based constitutive model and bp artificial neural network model in predicting high temperature flow stress of AZ80 magnesium alloy”, *Rare Metal Materials and Engineering*, v. 50, n. 11, pp. 3924–3933, Nov. 2021.
- [41] NAJM, H.T., AHMAD, N.S., AL-ARAJI, A.S., “Enhanced path planning algorithm via hybrid WOA-PSO for differential wheeled mobile robots”, *Systems Science & Control Engineering*, v. 12, n. 1, pp. 2334301, 2024. doi: <http://doi.org/10.1080/21642583.2024.2334301>.
- [42] WANG, F., ZHANG, H., LI, K., *et al.*, “A hybrid particle swarm optimization algorithm using adaptive learning strategy”, *Information Sciences*, v. 436, pp. 162–177, Apr. 2018. doi: <http://doi.org/10.1016/j.ins.2018.01.027>.
- [43] HAMEED, S., TANOLI, I.K., KHAN, T.A., *et al.*, “A novel self-healing genetic algorithm for optimizing single objective flow shop scheduling problem”, *Arabian Journal for Science and Engineering*, 2024. doi: <http://doi.org/10.1007/s13369-024-09240-x>.